Available online at www.sciencedirect.com
SCIENCE DIRECT
Journal of the European Ceramic Society 26 (2006) 201–208
www.elsevier.com/locate/jeurceramsoc

Variation of sintering parameters at an early stage of densification affecting β-Si_3N_4-microstructure

W. Lehner[a], H.-J. Kleebe[b,*], G. Ziegler[a]

[a] *Institute for Materials Research (IMA I), University of Bayreuth, D-95440 Bayreuth, Germany*
[b] *Colorado School of Mines, Metallurgical and Materials Engineering Department, Golden, CO 80401, USA*

Received 30 September 2003; received in revised form 20 June 2004; accepted 3 October 2004
Available online 21 December 2004

Abstract

The influence of sintering parameters at an early stage of densification on the evolution of a bimodal microstructure in Si_3N_4 ceramics was investigated. Commonly two different methods are pursued to design a bimodal Si_3N_4 microstructure: (i) annealing at a later sintering stage ($T > 1850\,^{\circ}C$) initiating β-Si_3N_4 grain growth via Ostwald ripening and (ii) seeding with β-Si_3N_4 nuclei, which abnormally grow during the liquid-phase sintering process. In this study, a third and novel method to design Si_3N_4 microstructures by affecting intrinsic nucleation phenomena at an early sintering stage is presented. In order to study the influence of sintering parameters on β-Si_3N_4 nuclei formation during the early stage of densification, temperature and pressure were systematically changed. Starting from identical green bodies (identical processing and doping), the variation of the sintering parameters affected intrinsic β-Si_3N_4 nucleation. This procedure allows variation in the fineness of the matrix as well as in the number and dimension of the large elongated β-Si_3N_4 grains embedded in the matrix. Since identical green bodies are used as starting material, the resulting microstructure can easily be tailored toward corresponding application needs.

Keywords: Grain growth; Microstructure-final; Si_3N_4; Sintering; Structural applications

1. Introduction

Potential application of silicon nitride in the field of tribology as ball bearings and in modern combustion engines offers the possibility of increasing efficiency and reducing energy consumption. This requires an improvement of material properties, particularly, with respect to the resistance against crack propagation.[1,2]

In contrast to a homogeneous fine grained matrix, a high aspect ratio of elongated Si_3N_4 grains in conjunction with a larger grain diameter leads to an improved *R*-curve behavior (e.g., $3\,MPa\,m^{1/2}$ versus $10\,MPa\,m^{1/2}$).[3–5] Mitomo et al.[10] reported a $\sqrt{2}$-correlation between fracture toughness and average grain diameter. Under the assumption of weak interface bonding, elongated grains embedded in a fine-grained matrix stimulate energy dissipation during crack propagation via crack deflection and elastic bridging.[6] Hence, a bimodal grain-size distribution is highly desirable.

One approach to this is the development of a bimodal microstructure, with elongated Si_3N_4 grains embedded in a fine and uniform matrix. Increased fracture toughness is attributed to the aforementioned mechanisms of crack deflection and elastic crack bridging. The formation of a bimodal microstructure is enhanced when using α-Si_3N_4 as starting powder.[7,8] The average aspect ratio of the β-Si_3N_4-grains in the final compound depends on the α–β-ratio in the Si_3N_4 starting powder.[9,10] Therefore, commercial Si_3N_4-ceramics are manufactured using powders with a high α-Si_3N_4 content. A large amount of β-Si_3N_4 accelerates the α–β-transformation during the liquid-phase sintering processs,[11–13] but typically yields a rather fine equiaxed microstructure. Doping with fine β-Si_3N_4-needles increases the number of elongated β-Si_3N_4-grains as well as their aspect ratio.[14–16] This leads to a highly bimodal microstructure and a rather effective reinforcement of Si_3N_4-ceramics.[17–20]

* Corresponding author.
E-mail address: hkleebe@mines.edu (H.-J. Kleebe).

0955-2219/$ – see front matter © 2004 Elsevier Ltd. All rights reserved.
doi:10.1016/j.jeurceramsoc.2004.10.015

A theoretical model to describe the α–β-transformation and its influence on microstructure evolution was presented by Krämer et al.[21] The degree of local supersaturation in the secondary glass phase is mainly controlled by three processes: (i) surface reaction between α-Si_3N_4 and glass melt (dissolution of α-Si_3N_4 particles), (ii) diffusion of Si_3N_4 through the secondary glass phase, and (iii) precipitation of Si_3N_4 on pre-existing or newly formed β-Si_3N_4 nuclei. Precipitation of solvated Si_3N_4 on β-Si_3N_4 nuclei is not the rate-determining step for the growth process.[22] Therefore, the degree of local supersaturation is only influenced by the first two mechanisms: reaction at the α-Si_3N_4/glass interface and diffusion through the melt. A variation of the heating rate during sintering affects the time-dependancy of (i) the solid/liquid reaction at the α-Si_3N_4 glass interface (dissolution; $\propto t$) and (ii) the diffusion through the glass ($\propto \sqrt{t}$). As a result, the probability of local supersaturation and, consequently, of nucleation increases with a lower heating rate. However, similar to the cast of a larger number of β-Si_3N_4-particles in the starting powder, a higher nucleation rate typically results in a relatively fine microstructure.

Data presented in the literature on homogeneous versus heterogeneous nucleation and on the effectiveness of interface reaction versus diffusion path are rather contradictory.[23–25] Hampshire and Jack[26] investigated the influence of different sintering additives such as Y_2O_3 and MgO on the development of the Si_3N_4 microstructure. They reported that densification of Y_2O_3-doped Si_3N_4 was mainly controlled by diffusion, while sintering MgO-doped Si_3N_4 was predominately affected by the α-Si_3N_4–glass interface reaction. Hence, no supersaturation occurred in the latter case and Si_3N_4 precipitated predominantly on pre-existing β-Si_3N_4 grains. On the other hand, Brook et al.[27] reported that densification and grain growth in MgO-doped Si_3N_4 was not affected by the solid/liquid interface kinetics, but was solely controlled by the diffusion through the secondary glass phase. They concluded that local nucleation of β-Si_3N_4 was in fact possible. In Y_2O_3-doped systems, the solvated material is congested in contact areas due to the higher glass viscosity. Consequently, the nitrogen concentration in the glass locally increased and Si_3N_4 crystallized as β-Si_3N_4 (homogeneous nucleaction). However, Lee et al.[28] reported that in Y_2O_3-doped SiAlON grain growth was independent from both volume fraction of glass and diffusion process. They concluded that in their system nucleation was most unlikely.

In general, homogenous nucleation takes place without the contribution of internal interfaces and is very probable when the secondary glass phase is highly supersaturated. In contrast, heterogeneous nucleation proceeds at α-Si_3N_4 interfaces. This nucleation mechanism occurs mainly in systems with a low volume fraction of glass and a high glass viscosity. Heterogeneous nucleation was described in the literature both for α′-SiAlON on α-Si_3N_4[29] and β′-SiAlON on β-Si_3N_4.[30] Braue et al.[31] reported on the heterogeneous epitaxy of silicon oxinitride, Si_2N_2O, on α-Si_3N_4.

Sajgalik und Galusek[32] studied the influence of amorphous Si_3N_4 addition on microstructure evolution. They observed that the microstructures became finer with increasing amount of amorphous Si_3N_4 and attributed this grain refinement to the formation of β-Si_3N_4 nuclei. Owing to the fast dissolution of amorphous Si_3N_4 in the glass phase, local supersaturation occurred initiating homogeneous nucleation.

One of the major problems to distinguish between homogeneous and heterogeneous nucleation is, however, to identify viable nuclei either as newly formed or as those that already existed in the Si_3N_4 starting powder. Therefore, nucleation events in the early stage of densification are commonly discussed in the literature based on phenomenological models. When the α–β-phase transformation is completed, further densification proceeds via dissolution of smaller and growth of larger β-Si_3N_4-grains (classical Ostwald ripening model). In the case of a diffusion-controlled Ostwald ripening process, abnormal grain growth of β-Si_3N_4 is strongly influenced by the chemistry of the secondary phase.[33] During the final sintering stage, microstructure coarsening is attributed to coalescence of β-Si_3N_4 grains.[34,35]

This paper describes the effect of different heating rates on the local supersaturation within the melt and, consequently, on the probability of β-Si_3N_4 nucleation. This process allows the manipulation of the number of nuclei affecting microstructure evolution. Moreover, an increase of the externally applied nitrogen gas pressure at an early stage of densification increases the number of large elongated β-Si_3N_4 grains formed upon densification. Variation of the sintering parameters, temperature and pressure, at an early stage of sintering (1400–1700 °C) can be employed for tayloring a highly bimodal microstructure.

2. Experimental procedures

Green bodies were prepared by aqueous slip casting. A commercial Si_3N_4-powder (Ube SN-E10) was used in this study. Sc_2O_3 (4 vol%) was added as sintering aid. The samples were sintered in a two-step gas-pressure sintering process (T_{max}: 1850 °C, p_{max}: 2 MPa). During sintering up to 1850 °C, the heating rate was varied. Different sintering cycles were employed, as illustrated in Figs. 1 and 2. An annealing step at low temperature (T: 1640 °C) was included into the sintering cycle. In addition, the applied N_2-pressure was increased to 1 MPa in the early stage of densification (Fig. 2). Moreover, the sintering process was interrupted at intermediate temperatures (1500–1850 °C), in order to characterize microstructure evolution.

The α–β-phase content was calculated by XRD-measurements (Seifert XRD 3000P; λ[Cu(K_α)]), using the ratio of intensity between the (2 1 0)-peak of the β-Si_3N_4-phase and the (2 1 0)-peak of the α-Si_3N_4-phase, [β/(α + β)].[36] The microstructure development upon sintering was characterized by SEM (Jeol JSM-6400, Jeol, Japan).

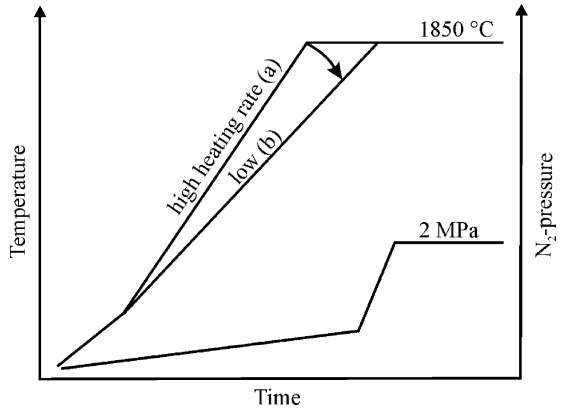

Fig. 1. Schematic of the two-step gas pressure sintering cycle with (a) high and (b) low heating rate at the early stage of densification.

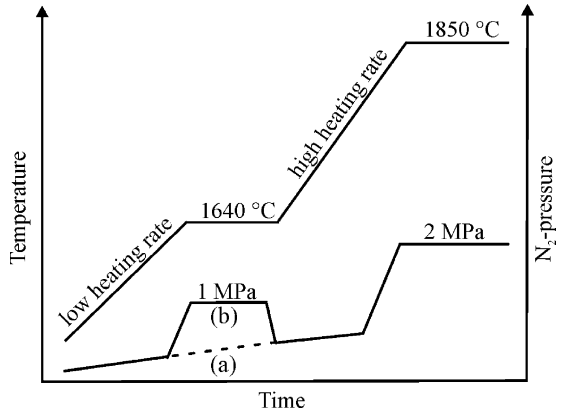

Fig. 2. (a) Introduction of an additional annealing step at 1640 °C and (b) increasing N_2-pressure at the early sintering state (schematic).

For this purpose, the surfaces were plasma-etched with CF_4-gas.

3. Results

3.1. Influence of different sintering parameters on α–β-phase transformation

When the sintering cycle was interrupted at 1580 °C, the SiO_2 localized at the α-Si_3N_4 surface had reacted with the sintering additive (Sc_2O_3) to form $Sc_2Si_2O_7$ and Sc_2SiO_5 (Fig. 3). The conversion of α-Si_3N_4 into the stable β-modification had already started. However the α–β-ratio still remained α-Si_3N_4 rich. In parallel, the reaction between Si_3N_4, SiO_2 and Sc_2O_3 had already taken place in the formation of Sc_2SiO_5 and Si_2N_2O, as given in Eq. (1). In Fig. 3, the different phase compositions depending on both sintering temperature and cycle are shown. At a temperature of 1680 °C, both transient phases, Si_2N_2O and Sc_2SiO_5, decompose and were not detected in the final microstructure at 1850 °C. The silicon oxynitride disintegrated into SiO_2

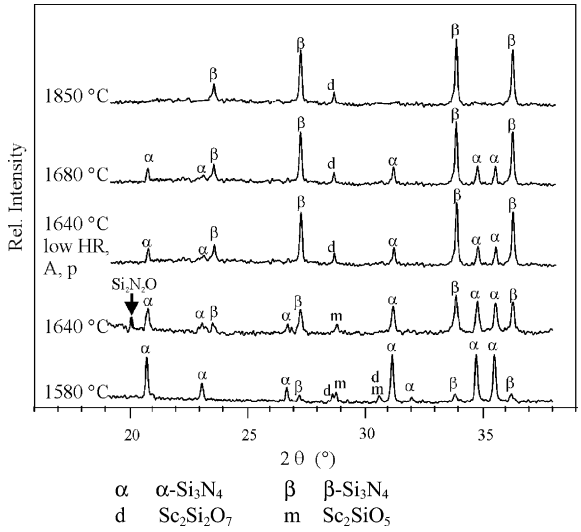

Fig. 3. XRD spectra of Si_3N_4 samples (interrupted sintering cycles) doped with 4 vol% Sc_2O_3; high heating rate (HR) at 1580, 1640, 1680 and 1850 °C. In addition, one spectrum was obtained at a low heating rate at 1640 °C, including an additional annealing step (A) and increased N_2-pressure (p).

and Si_3N_4 (Eq. (2)), while Sc_2SiO_5 reacted with the discharged SiO_2 to form the high-temperature stable $Sc_2Si_2O_7$ phase (see Eq. (3)). With increasing sintering temperature up to 1850 °C all α-Si_3N_4 was transformed into the β-modification.

$$Si_3N_4 + 2SiO_2 + Sc_2O_3 \rightarrow Sc_2SiO_5 + 2Si_2N_2O \quad (1)$$

$$2Si_2N_2O \rightarrow SiO_2 + Si_3N_4 \quad (2)$$

$$Sc_2SiO_5 + SiO_2 \rightarrow Sc_2Si_2O_7 \quad (3)$$

The reduction of the heating rate shifted the overall phase composition to that at higher temperatures. In addition, the α–β-phase transformation was accelerated with a reduced heating rate relative to the sintering temperature. No oxynitride but some $Sc_2Si_2O_7$ was detected at the sintering cycle interrupted at 1640 °C with a low heating rate (Eqs. (2) and (3); Fig. 3). The XRD-result was similar to that of an interruption temperature of 1680 °C and a high heating rate. Note that the introduction of an additional annealing step (A) with a higher N_2-partial pressure (p) resulted in a phase composition comparable to the sample sintered with a low heating rate and no increased p_{N_2}-pressure. In addition, the ds–dt-curve, determined by in-situ dilatometer measurement, shifted towards lower temperatures when a sintering cycle with a lower heating rate was applied (Fig. 4; $\Delta T = 60$ °C). It is assumed that the formation of the liquid glass melt occurred earlier (kinetic effect). Hence, particle rearrangement and α-Si_3N_4 solvation were initiated at a lower temperature. Consequently, the α–β-phase transformation was faster at a slow heating rate, as compared to a high heating rate relative to the sintering temperature (Fig. 5).

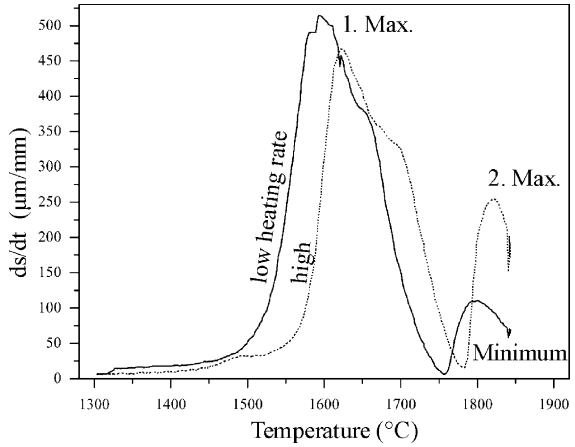

Fig. 4. Dilatometer curves (d*s*–d*t*) obtained with different heating rates, 4 vol% Sc_2O_3-doped Si_3N_4.

3.2. Microstructure development with different sintering parameters at an early sintering stage

The grain size of the densified bodies ($\rho > 97\%$ t.d.; T_{max}: 1850 °C) depends on the applied heating rate. A lower heating rate increased the number of small grains and decreased the average grain diameter. By comparing the SEM-micrographs of identical Si_3N_4-samples doped with 4 vol% Sc_2O_3 but sintered at different heating rates, a pronounced variation of the overall microstructure was observed (compare Figs. 6 and 7). A lower heating rate reduces the average particle diameter and the microstructure becomes in general finer. The number of large grains with a diameter of ≥5 μm markedly decreased. The SEM image in Fig. 8 illustrates the resulting microstructure after the incorporation of an additional annealing step (lower heating rate) at the d*s*–d*t*-maximum (1640 °C). With this variation of the sintering cycle at an early sintering stage, the microstructure became even finer, as compared to a sole lowering of the heating rate.

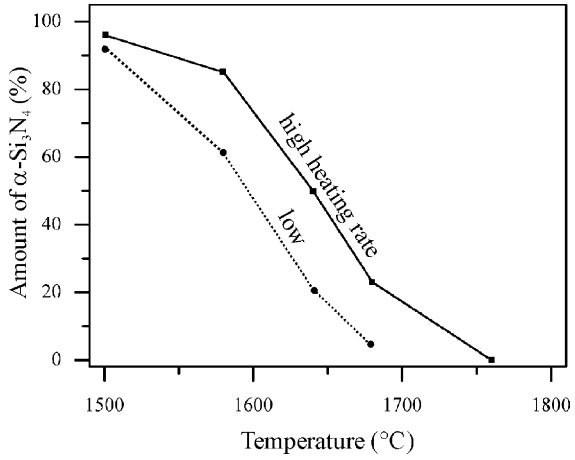

Fig. 5. Volume fraction of α-Si_3N_4 vs. temperature at different heating rates, 4 vol% Sc_2O_3-doped Si_3N_4.

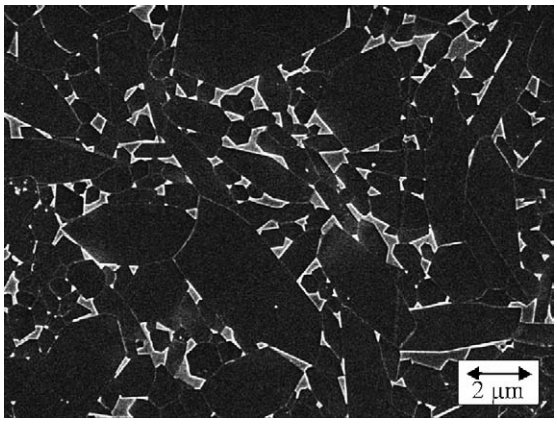

Fig. 6. SEM-micrograph of a 4 vol% Sc_2O_3-doped Si_3N_4; 1850 °C, high heating rate (see Fig. 1a).

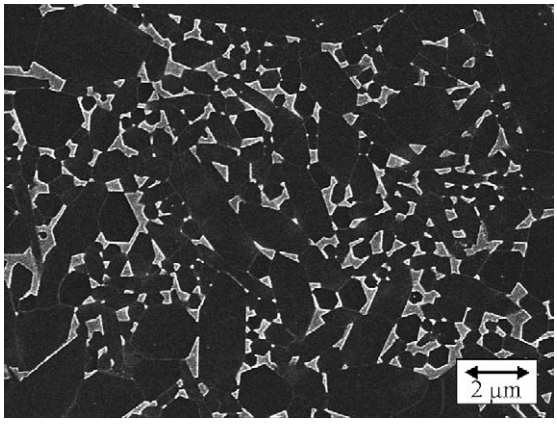

Fig. 7. SEM-micrograph of a 4 vol% Sc_2O_3-doped Si_3N_4, 1850 °C, low heating rate (see Fig. 1b).

In addition to the temperature profile the pressure program was varied (see Fig. 2b). The aim was to study how an increased N_2-partial pressure influences microstructure evolution, in particular, at the early stage of densification. Highly elongated β-Si_3N_4-grains embedded in a very fine-grained matrix were the result of this additional change in

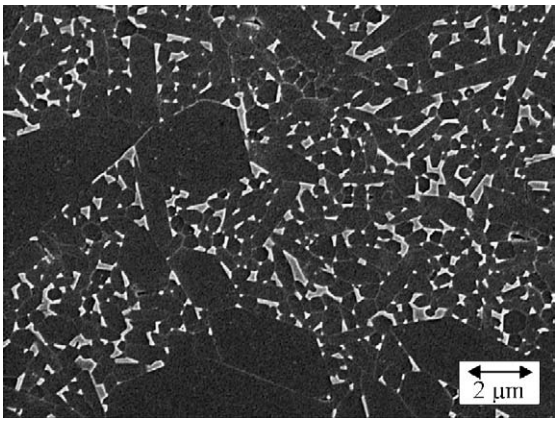

Fig. 8. SEM-micrograph of a 4 vol% Sc_2O_3-doped Si_3N_4, 1850 °C, low heating rate, additional annealing at 1640 °C (see Fig. 2a).

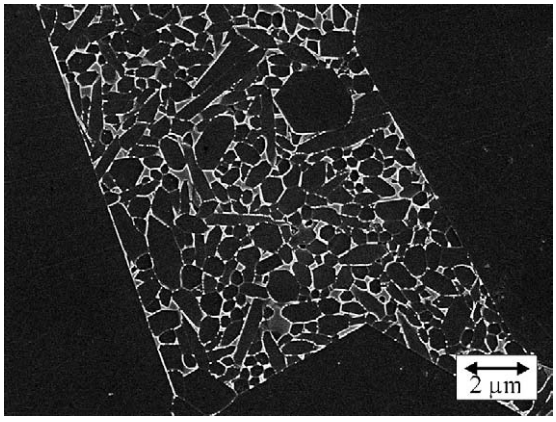

Fig. 9. SEM-micrograph of a 4 vol% Sc_2O_3-doped Si_3N_4, 1850 °C, low heating rate, annealing at 1640 °C in addition to increasing N_2-partial pressure (see Fig. 2b). Note that this is the most bimodal microstructure obtained by simply changing sintering conditions in the early stage of densification affecting nucleation and growth.

sintering atmosphere. The microstructure shown in Fig. 9 reflects the most bimodal grain-size-distribution achieved by simply varying the sintering parameters at an early sintering stage (compare Figs. 6 and 9).

4. Discussion

4.1. Nucleation process and influence of different heating rates

Liquid-phase sintering is controlled by two main processes: (i) reaction at the solid/liquid interface of the α-Si_3N_4 grains and (ii) diffusion of the solvated material through the secondary liquid phase (Fig. 10). Which mechanism dominates, primarily depends on the velocity of the diffusion process. If the diffusion is fast enough to transport all solvated Si_3N_4 from the α-Si_3N_4-surface to pre-existing β-Si_3N_4-grains, no supersaturation within the secondary phase will occur. In this case, the concentration changes little and the interface reaction is the time-dependent step for the α–β-phase transformation. Only pre-existing β-Si_3N_4-grains can grow under these conditions. However, if the diffusion process is slower than the dissolution of Si_3N_4, solvated Si_3N_4 locally enriches within the secondary phase (with prolonged reaction time) and nucleation becomes more probable (Fig. 11).

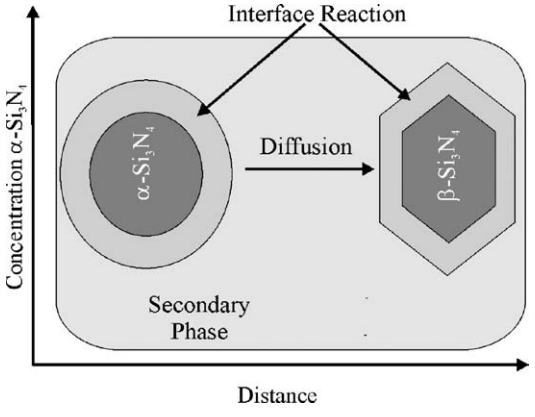

Fig. 10. Schematic showing the interface reaction vs. the diffusion process that occurs during the α–β-phase transformation.

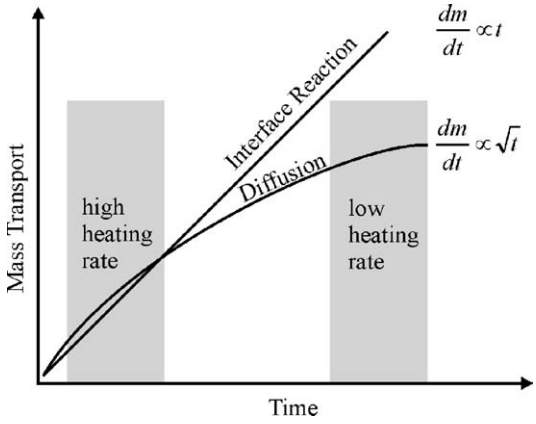

Fig. 11. Time dependency of interface reaction vs. diffusion at different heating rates. In the case of a lower heating rate nucleation of β-Si_3N_4 is more probable.

The general description of nucleation phenomena based on classical thermodynamic models reaches its limit when applied to Si_3N_4. β-Si_3N_4 nucleation takes place during sintering at elevated temperature, and is overlayed by the change in Si_3N_4 modification. During α–β-transformation, the system is in a non-steady state equilibrium. Theoretic formulations based on thermodynamic approaches can hardly explain this non-equilibrium state. An extension of the classical nucleation theory was introduced by Cahn and coworkers.[37–39] The description is based on the theory borrowed from continuum mechanics. The melt is treated as individual small volume elements, so-called clusters,[40–42] where every cluster is assigned a temperature and concentration. By this method, the cluster energy, E_{cluster}, of each volume element can be calculated as given in Eq. (4):

$$E_{\text{cluster}} = \int_V [f_{\text{ch}} - K^*(\nabla c)^2]\mathrm{d}V \tag{4}$$

where f_{ch} is the energy density of one volume element (which depends on the Si_3N_4 concentration within the secondary phase), E_{cluster} is the total energy of the volume element, K^* is a constant (varies between 19 and 100 J/m), and ∇c is the concentration gradient. The different clusters are able to interact with each other to exchange material or energy. The driving force is this attainment of a homogeneous distribution of both parameters, concentration and temperature, within the entire melt volume. The concentration gradient, ∇c, determines whether the cluster absorbs ($\nabla c < 0$) or desorbs ($\nabla c > 0$) material. Given a high concentration gradient, the different clusters have relatively low energies as compared to their next neighbors.

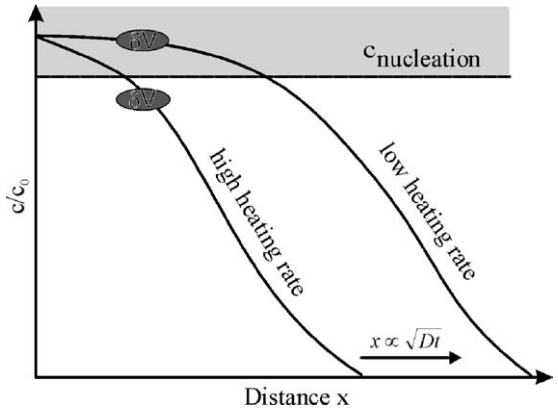

Fig. 12. Schematic description of the diffusion profile with different heating rates and their influence on nucleation. The diffusion profiles were calculated by the second Fick's law.

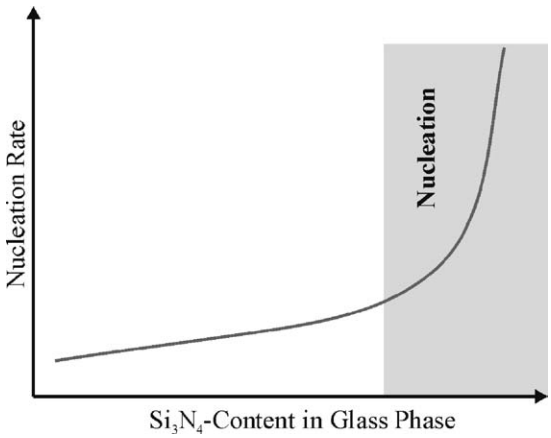

Fig. 13. Dependence of nucleation rate on local Si_3N_4 concentration in the secondary glass phase (Eq. (5)).

The driving force for the entire system is to achieve a homogeneous energy distribution. This leads to an energy transfer between different clusters. Consequently, ∇c decreases and $E_{cluster}$ increases, which is the requirement for nucleation. The necessary energy can be calculated from ΔE, the difference between the lattice energy and the cluster surface energy. With increasing ΔE the nucleation rate increases, as shown in Eq. (5):

$$N = N_0 \left[e^{\left(\frac{\Delta E}{kT}\right)} \right] \quad (5)$$

with N being the nucleation rate, k the Boltzmann constant, T the temperature, and N_0 is the nucleation rate at thermodynamical equilibrium.

Lowering the heating rate increases the nitrogen concentration near the surface of the α-Si_3N_4-grains (Fig. 12). At the same time, the diffusion front moves further into the secondary liquid phase. As a result, a lower concentration gradient develops. In comparing two volume elements within the same distance from an α-Si_3N_4-particle, a higher energy density, f_{ch}, and a lower concentration gradient, ∇c, would result in a sample densified at a lower heating rate. As a consequence of these two behaviors, a higher $E_{cluster}$ and ΔE would be observed which leads to an increased nucleation rate. Therefore, the reduction in heating rate resulted in the formation of a fine-grained microstructure in the Sc_2O_3-doped Si_3N_4 studied here. This effect can be explained by a higher concentration of solvated Si_3N_4 in the secondary phase and an increased probability of nuclei formation. In other words, the number of crystallites that can potentially grow rises and leads to a fine-grain microstructure.

The influence of annealing at early sintering stages on nucleation and grain growth can be rationalized in a similar way: With a reduced heating rate, a higher concentration of solvated Si_3N_4 within the secondary phase is generated. This is combined with a higher nucleation rate (Fig. 13). Without this additional annealing step at 1640 °C, a fraction of smaller nuclei would be dissolved during the continuous increase in sintering temperature because of the Gibbs–Thomson effect. Therefore, a reduced heating rate in addition to the incorporation of an annealing step (A) stabilizes a higher number of β-Si_3N_4-nuclei, resulting in a finer Si_3N_4 microstructure upon complete densification.

As shown in Fig. 8, the introduction of an annealing step at 1640 °C creates a fine microstructure. A remarkable difference in the amount of small grains with a size of <0.5 μm was observed. The finest microstructure was observed with the incorporation of an additional annealing step at 1640 °C. The maximum of the α–β-phase transformation is situated near this temperature (see Figs. 4 and 5). A fast α–β-transformation rate in conjunction with a low diffusion rate is the best assumption for the high local concentration of solvated Si_3N_4 ($>c_{nucleation}$) within the secondary phase and the corresponding increase in nucleation rate. During annealing the supersaturation decreases. As a result, no new nuclei are formed; instead stabilization of β-Si_3N_4 nuclei takes place and nuclei with smaller radii grow to overcritical crystallites. The result is an even finer microstructure in comparison to that resulting from simply lowering the heating rate.

In addition to the temperature profile, the N_2-pressure program was varied by continuously raising the pressure during the early sintering stage (maximum N_2-pressure = 1 MPa). The nitrogen partial pressure does not influence nucleation directly. Nucleation is in fact independent of the applied pressure, but is affected by it indirectly. During heating, more nitrogen is incorporated into the secondary liquid phase. Nitrogen transport predominantly occurs through the open porosity of the partially densified Si_3N_4 body. The incorporation of nitrogen into the residual glass network (not dissolved as molecular nitrogen) markedly increases the glass viscosity. As a result, the diffusion rate is lowered and the concentration of solvated Si_3N_4 increases continuously, further increasing the probability of β-Si_3N_4 nucleation (Fig. 13). Moreover, a higher N_2-partial pressure reduces the vapor pressure of smaller Si_3N_4 particles due to the Gibbs–Thomson effect. Besides nucleation, a stabilization of smaller nuclei is supported

in this manner. By changing the sintering parameters in the early stage of densification (heating rate, additional annealing step, nitrogen partial pressure), a very fine microstructure can be tailored with large ($\geq$10 μm diameter (Fig. 9)) elongated Si_3N_4-grains embedded in the fine-grain matrix. It is assumed that the increased nitrogen partial pressure also strongly favors the growth of pre-existing β-Si_3N_4 grains. This microstructure is by far the most bimodal microstructure achieved by simply varying the sintering parameters at an early stage of densification.

5. Conclusions

Variation of the sintering parameters, particularly at an early stage of densification, markedly affects microstructure evolution of Sc_2O_3-doped Si_3N_4. By (i) lowering the heating rate, (ii) introducing an additional annealing step and (iii) increasing the N_2-partial pressure within the temperature range of 1550–1700 °C, nucleation of β-Si_3N_4-nuclei is strongly enhanced, which results in a very fine-grained β-Si_3N_4 matrix. In addition, pre-existing β-Si_3N_4 particles showed considerable grain growth when subjected to this altered sintering program. Consequently, a highly aniosotropic microstructure with large elongated β-Si_3N_4-grains embedded in a rather fine matrix can be produced simply by tuning the sintering parameters at the early stage of densification. It is expected that such bimodal microstructures may reveal the synergistic effect of high strength and improved fracture toughness. Moreover, since identical green bodies can be utilized in this process, the creation of tailored microstructures that meet specific application needs becomes possible.

Acknowledgements

We greatly acknowledge the German Science Foundation (Deutsche Forschungsgemeinschaft (DFG); Bonn, Germany) for their financial support throughout this research. We would also like to thank B. Martin, University of Bayreuth, Germany, for his support during gas-pressure sintering and in situ dilatometry.

References

1. Riley, F. L., Silicon nitride and related materials. *J. Am. Ceram. Soc.*, 2000, **83**, 245–265.
2. Ziegler, G., Heinrich, J. and Wötting, G., Review: relationships between processing, microstructure, and properties of dense and reaction-bonded silicon nitride. *J. Mater. Sci.*, 1987, **22**, 3041–3086.
3. Ohji, T., Hirao, K. and Kanzaki, S., Fracture resistance behaviour of highly anisotropic silicon nitride. *J. Am. Ceram. Soc.*, 1995, **78**, 3125–3128.
4. Li, C. W., Lee, D. J. and Lui, S. C., *R*-curve behaviour and strength for in-situ reinforced silicon nitrides with different microstructures. *J. Am. Ceram. Soc.*, 1992, **75**, 1777–1785.
5. Li, C. W. and Yamanis, J., Super-tough silicon nitride with *R*-curve behavior. *Ceram. Eng. Sci. Proc.*, 1989, **10**, 632–645.
6. Faber, K. T. and Evans, A. G., Crack deflection processes—I. Theory. *Acta Metal. Mater.*, 1983, **31**, 565–576.
7. Lee, C. J., Kim, D. J. and Kang, E. S., Effect of α-Si_3N_4 particle size on the microstructural evolution of Si_3N_4 ceramics. *J. Am. Ceram. Soc.*, 1999, **82**, 753–756.
8. Okamoto, Y., Hirosaki, N., Akimune, Y. and Mitomo, M., Influence of α to β phase transformation on grain growth rate of silicon nitride. *J. Ceram. Soc. Jpn.*, 1997, **105**, 476–478.
9. Lange, F. F., Fracture toughness of Si_3N_4 as a function of the initial α-content. *J. Am. Ceram. Soc.*, 1979, **62**, 518–522.
10. Mitomo, M., Tsutsumi, M., Tanaka, H., Uenosono, S. and Saito, F., Grain growth during gas-pressure sintering of α-silicon nitride. *J. Am. Ceram. Soc.*, 1990, **73**, 2441–2445.
11. Sajgalik, P., α/β-Phase transformation of Si_3N_4 without sintering additives. *J. Eur. Ceram. Soc.*, 1991, **8**, 21–27.
12. Lu, H. and Huang, J., Microstructure in silicon nitride containing β-phase seeding: Part I. *J. Mater. Res.*, 1999, **14**.
13. Mitomo, M., Hirotsuru, H., Suematsu, H. and Nishimura, T., Fine-grained silicon nitride ceramic prepared from β-powder. *J. Am. Ceram. Soc.*, 1997, **78**, 211–214.
14. Mitomo, M., Yang, N., Kishi, Y. and Bando, Y., Influence of powder characteristics on gas-pressure sintering of Si_3N_4. *J. Mater. Sci.*, 1988, **23**, 3412–3419.
15. Park, D., Choi, M., Roh, T., Kim, H. and Han, B., Orientation-dependant properties of silicon nitride with aligned reinforcing grains. *J. Mater. Res.*, 2000, **15**, 130–135.
16. Hirosaki, N., Akimune, Y. and Mitomo, M., Microstructure characterisation of gas-pressure-sintered β-silicon nitride containing large β-silicon nitride seeds. *J. Am. Ceram. Soc.*, 1994, **77**.
17. Hoffmann, M. J., Analysis of microstructural development and mechanical properties of Si_3N_4 ceramics. In *Tailoring of Mechanical Properties of Si_3N_4 Ceramics*, ed. M. J. Hoffmann and G. Petzow. Kluwer Academic Publication, 1994, pp. 59–72.
18. Wittmer, D. E., Doshi, D. and Paulson, T. E., Development of β-Si_3N_4 for self reinforced composites. In *Proceedings of the Fourth International Symposium on Ceramic Mater. and Components for Engines*, ed. R. Carlsson, T. Johansson and L. Kahlmann. Elsevier Appl. Science Publ., 1992, pp. 594-02.
19. Hirao, K., Nagaoka, T., Brito, M. E. and Kanzaki, S., Microstructure control of silicon nitride by seeding with rodlike β-silicon nitride particles. *J. Am. Ceram. Soc.*, 1994, **77**, 1857–1862.
20. Kanzaki, S., Brito, M. E., Valecillos, M., Hirao, K. and Toriyama, M., Microstructure designing of silicon nitride. *J. Eur. Ceram. Soc.*, 1997, **17**, 1841–1847.
21. Krämer, M., Hoffmann, M. J. and Petzow, G., Grain growth of Si_3N_4 during α/β-transformation. *Acta Metal. Mater.*, 1993, **41**.
22. Okamoto, Y., Hirosaki, N., Akimune, Y. and Mitomo, M., Influence of α to β phase transformation on grain growth rate of silicon nitride. *J. Ceram. Soc. Jpn.*, 1997, **105**, 476–478.
23. Hwang, C. J. and Tien, T.-Y., Microstructural development in silicon nitride ceramics. *Mater. Sci. Forum*, 1989, **47**, 84–109.
24. Wötting, G. and Ziegler, G., Influence of powder properties and processing conditions on microstructure and mechanical properties of sintered Si_3N_4. *Ceram. Int.*, 1984, **10**, 18–22.
25. Messier, D. R., Riley, F. L. and Brook, R. J., The α/β silicon nitride phase transformation. *J. Mater. Sci.*, 1978, **13**, 1199–1205.
26. Hampshire, S. and Jack, K. H., Densification and transformation mechanisms in nitrogen ceramics. In *Nitrogen Ceramics*, ed. F. L. Riley. Martin Nijhoff Pub., Boston, 1983, pp. 226–235.
27. Brook, R. J., Carruthers, T. G., Bowen, L. J. and Weston, R. J., Mass transport in the hot pressing of α-silicon nitride. In *Nitrogen Ceramics*, ed. F. L. Riley. Noordhoff Int. Publ., Leyden, 1977, pp. 433–447.

28. Lee, D., Kang, S., Petzow, G. and Yoon, D., Effect of a to β (β′)phase transformation on the sintering of silicon nitride ceramics. *J. Am. Ceram. Soc.*, 1990, **73**, 767–776.
29. Hwang, S. L. and Chen, I. W., Nucleation and growth of α′-SiAlON on α-Si_3N_4. *J. Am. Ceram. Soc.*, 1994, **77**, 1711–1718.
30. Hwang, S. L. and Chen, I. W., Nucleation and growth of β′-SiAlON. *J. Am. Ceram. Soc.*, 1994, **77**, 1719–1728.
31. Braue, W., Pleger, R. and Luxem, W., Nucleation and growth of Si_2N_2O in Si_3N_4-materials employing different sintering additives. *Key Eng. Mater.*, 1994, **89–91**, 483–487.
32. Sajgalik, P. and Galusek, D., α–β-Transformation of silicon nitride: homogenous and heterogenous nucleation. *J. Mater. Sci.*, 1993, **12**.
33. Kleebe, H.-J., Pezzotti, G. and Ziegler, G., Microstructure and fracture toughness of Si_3N_4 ceramics: combined roles of grain morphology and secondary phase chemistry. *J. Am. Ceram. Soc.*, 1999, **82**, 1857–1867.
34. Kaysser, W. A., Takajo, S. and Petzow, G., Particle growth by coalecence during liquid phase sintering of Fe–Cu. *Acta Metal. Mater.*, 1984, **32**, 115–122.
35. Takajo, S., Kaysser, W. A. and Petzow, G., Analysis of particle growth by coalescence during liquid phase sintering. *Acta Metal. Mater.*, 1984, **32**, 107–113.
36. Gazzara, C. P. and Messier, D. R., Determination of phase content of Si_3N_4 by X-ray diffraction analysis. *Am. Ceram. Soc. Bull.*, 1977, **56**, 777–781.
37. Cahn, R. W., Haasen, P., Kramer, E. J. and Kampmann, R., ed., *Homogeneous Second Phase Precipitation in Mat. Science and Technology: Phase Transformation in Materials*. VCH-Verlag, 1991, pp. 242–269.
38. Hillert, M., On the theory of normal and abnormal grain growth. *Acta Metal. Mater.*, 1965, **13**, 227–238.
39. Hellmann, P. and Hillert, M., On the effect of second-phase particles on grain growth. *Scand. J. Metal.*, 1975, **4**, 211–219.
40. Binder, K., Stauffer, D. and Krumbhaar, H. M., Calculation of dynamic critical properties from a cluster-reaction theory. *Phys. Rev. B*, 1974, **10**, 3853–3857.
41. Binder, K. and Stauffer, D., Statistical theory of nucleation, condensation and coagulation. *Adv. Phys.*, 1976, **25**, 343–396.
42. Binder, K., Stauffer, D. and Krumbhaar, H. M., Theory for the dynamics of clusters near the critical point. I. Relaxation of the Glauber kinetic ising model. *Phys. Rev. B*, 1975, **12**, 5261–5287.